Spaceborne GNSS-Reflectometry on TechDemoSat-1: Early Mission Operations and Exploitation

Martin Unwin, Philip Jales, Jason Tye, Christine Gommenginger, Giuseppe Foti, and Josep Rosello

***Abstract*—GNSS-Reflectometry is a new technique that shows promise for many earth observation applications including remote sensing of oceans, land, and ice. A payload has been developed that is low size and power, and suitable for use on small satellites. The first flight of the SGR-ReSI GNSS Reflectometry Instrument is on the TechDemoSat-1 mission, launched in July 2014. The instrument has been operational since its commissioning in September 2014, and has been collecting delay Doppler maps routinely over many different surfaces. Preliminary work has been undertaken to develop and validate wind speed inversion algorithms against ASCAT measurements with promising results. Measurements over land and sea ice are also showing interesting geophysical characteristics This paper describes the instrument, early operations, data dissemination through the Measurement of Earth Reflected Radionavigation Signals By Satellite (MERRByS) website and preliminary data assessments in preparation for further data exploitation.**

***Index Terms*—GNSS reflectometry, GNSS remote sensing, mean-square slope, sea-state sensing, signal processing, techdemosat TDS-1.**

I. Introduction

THE GPS Reflectometry experiment on the UK-DMC satellite mission, launched in 2003, proved the feasibility of using GNSS reflections for measuring the sea state and other geophysical observables through a partnership between SSTL and National Oceanography Centre (NOC) [1]–[3]. Subsequently, a new instrument was developed called the Space GNSS Receiver Remote Sensing Instrument (SGR-ReSI) to gather more spaceborne reflectometry data and demonstrate the potential for a sea-state service. The first opportunity arose for the flight on a satellite called TechDemoSat-1 (TDS-1) initiated in 2010, and with the launch taking place in July 2014.

In parallel, a US mission called CYGNSS was selected by NASA that plans to measure hurricanes with reflected GNSS signals collected using an updated revision of the SGR-ReSI, (also referred to as delay Doppler mapping Instrument) as payload on each of the eight satellites. This project is led by University of Michigan and prime contractors are South West Research Institute, and satellites are due for launch in 2016–17 [4].

This paper describes the instrument on TDS-1, early operations and preliminary data review in preparation for the data exploitation campaign.

Manuscript received April 13, 2016; revised May 31, 2016 and August 12, 2016; accepted August 16, 2016. Date of publication September 27, 2016; date of current version October 14, 2016. This work was supported in part by under European Space Agency under contract 4000109726. Previous support for instrument development and TDS-1 came from ESA, the Centre for Earth Observation and Instrumentation, InnovateUK, SEEDA, UKSA, NERC and Surrey Satellite Technology Ltd. *(Corresponding author: Martin Unwin.)*

M. Unwin and P. Jales are with the GNSS Team, Surrey Satellite Technology Ltd., Guildford GU2 7YE, U.K. (e-mail: m.unwin@sstl.co.uk; p.jales@sstl.co.uk).

J. Tye is with the Surrey Space Centre, University of Surrey, Guildford GU2 7XH, U.K. (e-mail: j.tye@surrey.ac.uk).

C. Gommenginger is with the Ocean Observing and Climate, National Oceanography Centre, Southampton SO14 3ZH, U.K. (e-mail: c.gommenginger@noc.soton.ac.uk).

G. Foti is with the Satellite Oceanography, National Oceanography Centre, Southampton SO14 3ZH, U.K. (e-mail: g.foti@noc.ac.uk).

J. Rosello is with the Earth Observation Directorate, European Space Research and Technology Centre, Noordwijk SO14 3ZH, The Netherlands (e-mail: Josep.Rosello@esa.int).

Color versions of one or more of the figures in this paper are available online at http://ieeexplore.ieee.org

Digital Object Identifier 10.1109/JSTARS.2016.2603846

II. Motivation for Work

Oceanographers have learnt over time how to exploit measurements from spaceborne microwave radars and radiometers as inputs into ocean and atmospheric models; altimeters such as GEOSAT, Topex-Poseidon and the Jason series, SAR on ERS and Envisat, and scatterometers on ERS and QuikSCAT have all been used to provide regularly updated information about the sea surface, wind, and wave conditions that are of value to near-real time applications and to build long-term legacy data in support of climate research. While the measurements these satellites provide are highly valued, the sampling they offer remains limited compared to the forever growing demand for 24/7 operation, global coverage, and higher temporal and spatial resolution. The best sampling, provided by scatterometers, remains limited to daily global coverage. Altimeters have narrow ground tracks with repeat visits ranging from 10 to 35 days. Sea state and wind conditions on the ocean can change dramatically within a few hours, sometimes within minutes, in temporal terms, and within a few km in spatial terms, particularly near high-intensity weather systems or in coastal regions. Fine scale temporal and spatial variability is not sampled, and scientists know that many processes at the sea surface are just not being observed.

Recently, there has been a widespread recognition that more work is needed to ensure this missing information can be measured [5], with high-density sampling and timeliness being recognized as important for many operational applications such as forecasting and disaster risk management [6]. Several wide swath satellite concepts have been proposed that should help address these needs, and there are proposals to use satellite constellations to increase the sampling and coverage. To enable a constellation, it is necessary to find payloads that are relatively

TABLE I
POTENTIAL APPLICATIONS FOR GNSS REFLECTOMETRY

Domain	Applications
Sea state and ocean winds	Meteorology, climate models, commercial services for waves and wind, shipping, offshore exploration, renewable energy, . . .
Sea surface height	Geostrophic currents, mesoscale eddy monitoring
Ice edge location Ice and snow	Ice edge, ice concentration, freeboard height, snow depth, snow melt
Land reflections	Soil moisture, biomass
Atmosphere	Technology has close link with GNSS Radio Occultation techniques

small, simple, and low cost such that they can be manufactured in quantity and offered at an affordable price to the user community.

The development of the SGR-ReSI was primarily aimed at addressing the need for sea-state determination, although other applications were also identified as secondary objectives. Other potential future applications are listed in Table I that are under consideration.

In this study, we show how the preliminary GNSS-R data from TechDemoSat-1 has been collected, processed, and validated against other sources of wind speed. Furthermore, a ground-processing chain has been put in place to invert the data and produce simple wind speed products that are made available to users via a web-based server in a form that could be a blueprint for a future near-real time weather-/sea-state data service.

III. SGR-RESI ON TDS-1

The technology demonstration satellite, TechDemoSat-1 (TDS-1) is a satellite intended to provide an early flight for UK space technology with a view to promoting future use. The satellite was built by SSTL under sponsorship of the UK Space Agency and the Technology Strategy Board and with contributions from the payload suppliers.

A. *TechDemoSat-1*

TechDemoSat-1 (see Fig. 1) is based upon a standard SSTL design, the SSTL-150. With its eight payloads, the satellite is approximately 160 kg. It is capable of accommodating around 52 w of orbit-average power and can store up to 128 GBytes of payload data. It has S-Band and X-Band downlinks capable of operating with experimental downlink speeds up to 400 MB/s. It has four-wheel slew agility, and new generation gyros, magnetometers, and torque rods.

The SGR-ReSI is one of the eight UK payloads hosted on TechDemoSat-1 (others including an altimeter, radiation, charge and atmospheric measuring instruments, and deorbit sail) alongside a number of new SSTL platform technology demonstrations. As a result of the multiple payloads, none are allowed to be operated continuously, but are allocated specific days on an eight-day operating cycle.

The two main purposes of the SGR-ReSI on TechDemoSat-1 are to demonstrate its core GPS capability, and to demonstrate the technology and science required for GPS Reflectometry

Fig. 1. TechDemoSat-1 (TDS-1) prior to launch.

Fig. 2. SGR-ReSI SGR-ReSI, part of sea-state payload on TDS-1.

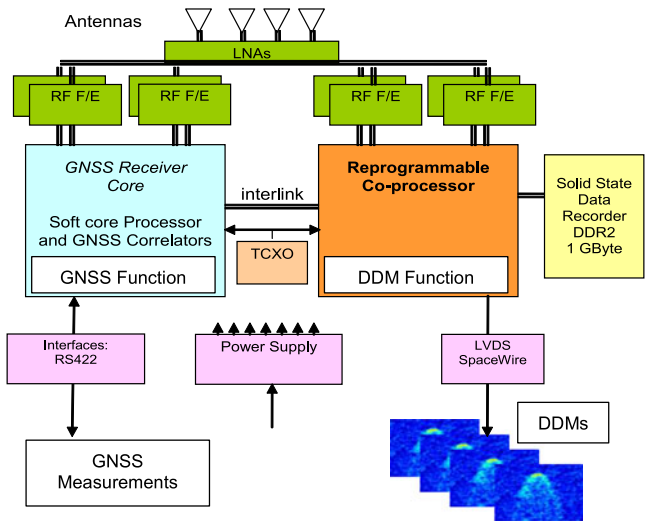

Fig. 3. SGR-ReSI GNSS-R architecture.

through the operation and collection of data over the ocean. Secondary aims include demonstration of some of the SGR-Axio's planned extra capabilities—such as multiconstellation and multifrequency operation.

B. *Space GNSS Receiver Remote Sensing Instrument*

The SGR-ReSI is shown in Fig. 2 while Fig. 3 shows the instrument architecture and the delay Doppler map (DDM) flow.

The GNSS receiver core is implemented on a flash-based FPGA (ProASIC-3), while the signal processing capability is

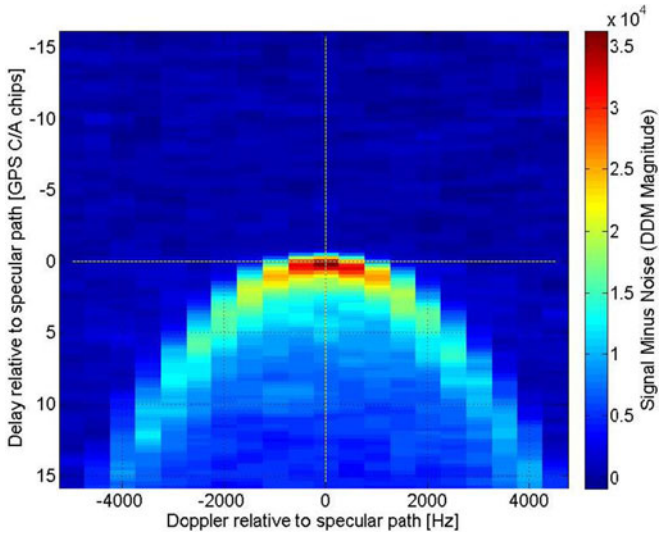

Fig. 4. Example DDMs from TDS-1.

provided by a second FPGA coprocessor which is controlled and configured from the ProASIC3. This is a Xilinx Virtex 4 FPGA which is based on SRAM, allowing the upload of new coprocessing algorithms even once the SGR is in orbit. It enables special processing algorithms for reflected or occulted signals used allowing the equivalent of thousands of corelators to map the distorted signals. To allow the storage of both sampled and processed data, a bank of DDR2 memory with a capacity of 1 GB is used.

The receiver supports the GPS L1 frequency band, but also carries reprogrammable frontends that can be set up at any of the navigation bands. Limitations are imposed by the choice of antennas and LNA filtering. Initially GPS L1 C/A signals are supported, but in future Galileo E1bc and Glonass are expected to be implemented in the VHDL and software.

The instrument supports multiple interfaces (CAN, RS422, USB, SpaceWire), so it could be accommodated by a variety of different satellite missions. The unit is around 1 kg in mass, consumes approximately 10 W, and fits within half of an SSTL standard satellite microtray (approx. $300 \times 160 \times 30$ mm^3).

The instrument is principally designed for a GNSS-R, using the ground-reflected GNSS signals to remotely sense the Earth's surface. Reflected GPS L1 signals are processed into DDMs, as shown in Fig. 4, either on-board using the coprocessor, or alternatively on the ground if the raw data is downloaded.

In the raw data mode, the sampled data from the RF frontends is stored into the on-board solid-state data recorder prior to download via the LVDS port; 1–4 min of raw data (depending on the number of RF channels sampled) can be stored before the 1 GB data recorder is full (typically recording at 160 Mb/s). In the second mode, algorithms in the coprocessor process the raw data into DDMs, based on work by Jales [7]. The DDMs are at a low enough data rate to permit continuous streaming of data (typically 320 kb/s).

For the coprocessor to generate DDMs of the sampled reflected data, it needs to be primed with the correct GPS satellite code (referred to as PRN), the estimated delay, and the

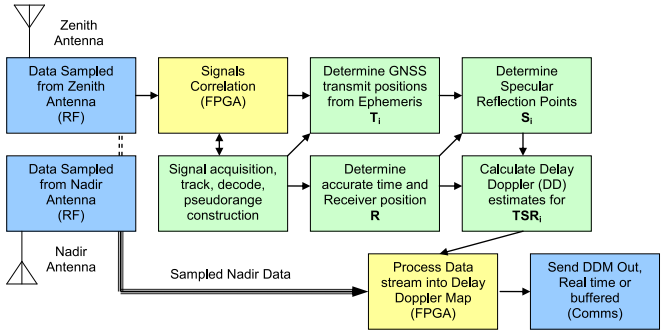

Fig. 5. Schematic representation of the GNSS-R DDM on-board processing flow.

estimated Doppler of the reflection as seen from the satellite. These are calculated by the processor in conjunction with the main navigation solution—the data flow for this is shown in Fig. 5. Direct signals (from the zenith antenna) are used to acquire and track GNSS signals. From the broadcast Ephemerides, the GNSS satellite positions are known. Then, from the geometry of the position of the user and the satellites, the reflectometry geometry can be calculated, and hence, an estimate of the delay and Doppler of the reflection.

A local replica of the GPS code is generated that is correlated against the incoming signal. In the case of a DDM, the delay and Doppler values are not controlled by a closed tracking loop, but are placed as a matrix of pixels across the spread reflected signal to form an image. The placement of these pixels is controlled by the prediction of the location of the reflected signals.

A mixture of a coherent integration and incoherent integration is used to receive weak signals as their phase coherency has been partially lost due to the motion over a rough surface (previous studies suggest 1 ms is about the maximum coherent integration period before destructive interference starts to dominate [8]).

As the signals are correlated, the bandwidth is reduced from the GPS L1 C/A code 2 MHz down to sub-kHz levels, which allows the separation of the signal components in the Doppler domain. Further speeding of the processing can be achieved by using a fast Fourier transform, allowing a single row of values to be calculated across the Doppler domain simultaneously (see Fig. 6).

A comparison of the capabilities of the GNSS-R instrument against a specific configuration on TDS-1 and CYGNSS missions is given in Table II.

C. SGR-ReSI Configuration on TDS-1

Although the SGR-ReSI can, in principle, support up to four dual-frequency antennas, a reduced subset is being flown on TechDemoSat-1 to support its planned applications. A left-hand circularly polarized dual-frequency L1/L2 fixed phased array antenna (gain 13.3 dBiC with approx. 30° half-power pattern at L1) sits on the earth facing facet for the GNSS reflectometry. It is the opposite polarization to conventional GNSS antennas and provides the higher gain required to receive the weak signals from GNSS reflections. A dual-frequency L1/L2 antenna and two additional L1 antennas occupy the space facing facet with

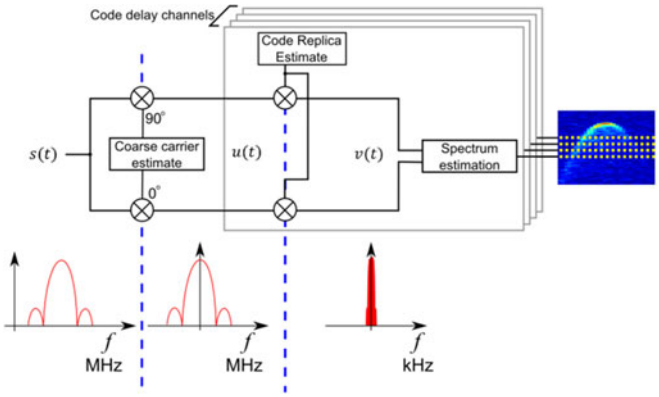

Fig. 6. Computation of DDM row through process of down conversion, modulation removal followed by spectrum estimation.

TABLE II
SGR-ReSI Instrument Characteristics

	Capability	TDS-1 configuration	CYGNSS configuration
Frequency capability	4 × L1, 4 × progr. (L2, E5, E6)	L1 and L2C	L1 only
GNSS	24 chan. L1, L2C Glonass Galileo Potential	24 chan. GPS L1 and L2C, Galileo E1	15 chan. GPS L1
Antenna ports	8 single or 4 dual frequency	1 nadir ant 3 zenith ant.	2 nadir ant (SF) 1 zenith antenna
Zenith Antenna		Dual freq, 3 dBi gain	Single Freq, 4 dBi gain
Nadir Ant.	(UK DMC was 11.8 dBi)	13.3 dBiC	14.5 dBic × 2
Nadir Offpointing	(UK DMC was 10 deg)	6° in –*X*-axis (L1)	Panels offpoint by 28°
LNA Noise Figure		2.7 dB dual freq	2.0 dB single freq
Sampling Rate	16.367 MHz up to 65.5 MHz I or I & Q, 2 or 2.5 bit	16.367 MHz I only, 2 bit	16.0362 MHz, I only
DDM Format	Block Floating Point	16 or 32 bit depth	32 bit depth
Default Pixels	Delay & Doppler can be reconfigured	128 × 250 ns 20 × 500 Hz)	128 × 250 ns 20 × 500 Hz
Co-Processor	Xilinx Virtex 4	V4-SX30	V4-LX60
Number of Reflections	4	4 (limited by antenna pattern)	4
Data rate of DDMs	Approx 320 kbps	Same	Same
Data logging	1 Gbyte	Same	Same
GPS Performance	Approx. 5 m, 10 cm/s	Same	Same
Size, Mass	300 × 200 × 50 mm, 2 kg	Same (in 1/2 microtray)	Same (in box)
Power	4 W in GNSS mode 9 W in DDM mode	Same	Same

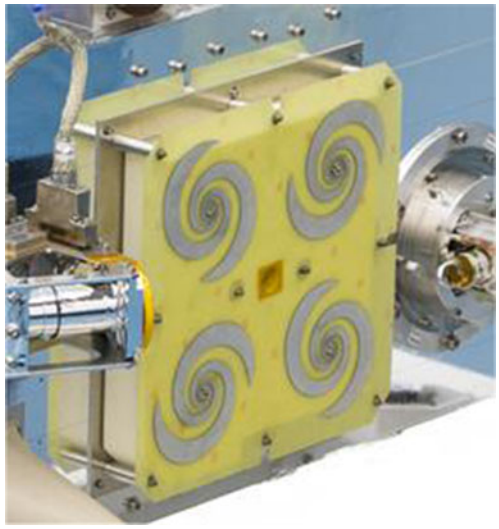

Fig. 7. TDS-1 Nadir GNSS antenna.

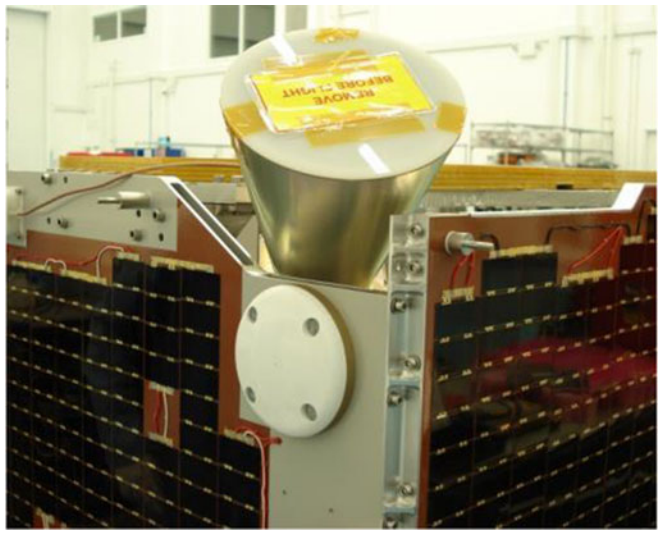

Fig. 8. TDS-1 Zenith GNSS antenna.

Fig. 9. TDS-1 GNSS dual frequency low noise amplifier.

more typical RHCP and hemispherical patterns. These antennas are intended to provide navigation function for the satellite. The provision of three antennas on the space facing facet with suitable baselines between them also enables the SGR-ReSI to support GNSS-based attitude determination as previously demonstrated by SSTL on the UoSAT-12 and TopSat satellites. Fig. 7 shows the high-gain nadir antenna and Fig. 8 the zenith antenna, both of which are dual frequency.

A low noise amplifier (see Fig. 9) was designed that supports both L1 and L2 frequencies, is equipped with a temperature sensor, and a switched load to provide a known noise level when enabled for calibration purposes. One each is used on the

TABLE III
NOMINAL TDS-1 ORBIT (OSCULATING ELEMENTS)

Element	Value
Semi-major axis	7009.44 km
Eccentricity	0.00059
Inclination	98.399°
Longitude of the ascending node	75.223°
Perigee argument	30.96°
Argument of latitude	216.325°
RAAN rate of change LTAN Drift	1.044°/Day 1.42 h/year

TABLE IV
TYPICAL TDS-1 TWO-LINE ELEMENT SET (11TH MARCH 2016)

1 40076U 14037H 16071.18046555 .00000359 00000-0 53524-4 0 9991
2 40076 98.3261 158.4172 0007090 114.8501 245.3454 14.81146800 90483

nadir and zenith dual-frequency antennas, respectively. The two L1-only zenith antennas have integrated L1 LNAs as used with previous single-frequency GNSS receivers.

Development and testing of this instrument is described in [9]. Further information on the SGR-ReSI and its configuration on TDS-1, including antenna patterns and LNA characteristics, is available from resources on the Measurement of Earth Reflected Radio-navigation Signals By Satellite (MERRByS) website [10].

IV. LAUNCH AND FIRST OPERATIONS

A. Launch

The Soyuz-2 launcher was successfully launched on 8th July 2014 and it deployed its main payload the Meteor-M №2 weather remote sensing satellite at an orbit of 825 km altitude, then after manoeuvres, the Fregat upper stage deployed all eight secondary payloads in a lower orbit, including TDS-1. It was injected successfully into its nominal orbit (see Table III).

The orbit processes slowly with time as it is not in a perfect sun-synchronous inclination, as a result of being a secondary launch payload. The latest orbit can be obtained from publically released NORAD tracking elements [11] using a catalogue identifier 40076. (See Table IV for example).

TDS-1 commenced life with local time of ascending node (LTAN) of 09:00, but is drifting to 12:00 over its three year life. A major consideration is how the TDS-1 drifting LTAN compares with that of other ocean wind and wave sensing missions, and how this affects the possibility of close temporal and spatial collocation with other satellites through the TDS-1 mission lifetime. The ASCAT scatterometer on MetOp-A has < 1 h crossover with TDS-1 at the beginning of its mission. The ASCAT sensor is carried on MetOp-A launched in 2006 and has a swath of 550 km (MetOp-B launched in 2012 has also been placed in the same orbit).

The launch and early operations phase for the satellite platform was completed on 25th July 2014 and payload commissioning then took place from July until October. As TDS-1 is a demonstration satellite with many new payloads, only a low level of commissioning was required on the basis that further payload experimentation and verification would be taking place throughout the mission. The SGR-ReSI was demonstrating both performances as a platform GNSS receiver and as a remote sensing payload, so testing started with the navigation performance prior to reflectometry operations.

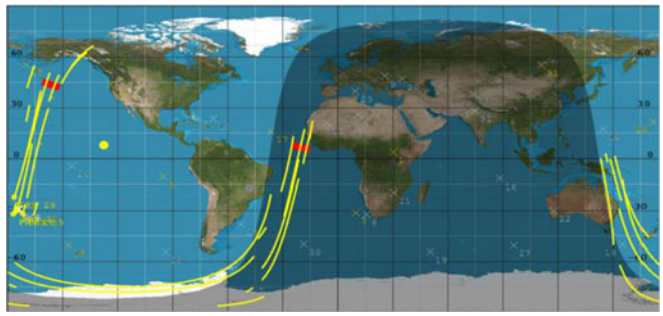

Fig. 10. Map of DDM collections (yellow tracks) and raw data captures (red blocks) obtained 01/09/2014.

Commissioning of the SGR-ReSI instrument began on 16th July 2014. The first operations consisted of an initial health check to ensure that the receiver was powering on and functioning correctly, followed by a single orbit of operation (around 1.5 h) during which the receiver was configured into its basic GPS only navigation mode and allowed to collect position, velocity, and time telemetry. A rapid acquisition and position fix was achieved, and preliminary orbit fitting indicated a self-consistency at the level of around 2.5 m. Following this, the receiver application software and coprocessor synthesized VHDL image were updated to the latest versions to enable reflectometry testing to begin.

B. First Reflectometry Operation

A number of minor spacecraft and instrument configuration issues needed to be addressed as part of the payload commissioning, but once these were resolved the reflectometry operations could commence. On the 1st September, there were two successful reflectometry operations—at 10:28 and 20:03 UTC, comprising of raw data collections and DDM collections.

These operations resulted in the following data being captured (see Fig. 10):

1) SGR Binary Packet Protocol log containing the packet-based telemetry generated by the SGR-ReSI.
2) Two raw data logs, each 1 m in duration containing raw sampled IF GPS L1 data from Antenna 1 and Antenna 2.
3) Two DDM collection logs containing a cumulative total of 4896 DDMs for each DDM channel, or 19 584 DDMs in total. Given that one DDM is generated every 1 s, this corresponds to about 81 min.

The generation of DDMs in these first hours of operations represented about four times the quantity (by time period) of DDMs generated in the entire lifetime of the UK-DMC experiment.

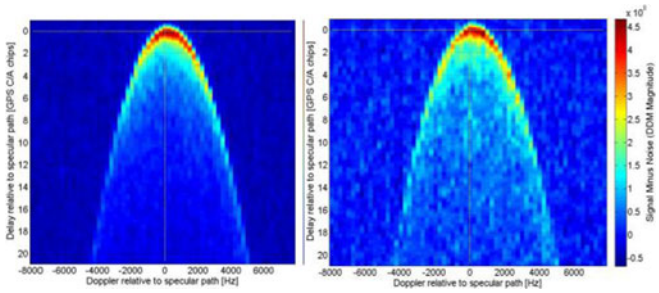

Fig. 11. GPS PRN 12 and 25 DDMs generated from 20:10 UTC raw data collection.

C. Raw Data Capture

The initial set of operations resulted in two raw data captures over open ocean, each 1 min in duration. The locations of the raw data captures are shown by the thick red tracks in Fig. 10 occurring at 10:28 UTC and 20:10 UTC, respectively. A software receiver on-ground was used to recover the DDMs of reflections from three different satellites. The signal quality appears to be at least as good as the DDMs recovered from UK-DMC. Fig. 11 shows the reflections from two of the three different GPS satellites recovered from within the sampled data, processed in this case with a coherent integration time of 4 ms, rather than the 1 msused on-board the instrument.

D. On-Board DDMs

The longer DDM file contained data from 10:34 UTC to 11:27 UTC and begins as the satellite was passing slightly west of Mauritania (on the west coast of Africa) and heading out over the Atlantic Ocean. Fig. 12 shows the position of the four reflections tracked by the SGR-ReSI at 10:34:49 UTC with a corresponding screen capture of the DDMs taken from the DDM playback tool. Each DDM has 20 pixels in y-axis (Doppler) and 128 pixels in the y-axis (delay) as described in Table II.

V. Data Structure, Collection, and Assessment

A. Product Levels

Although DDMs are processed on-board the TDS-1 SGR-ReSI in orbit, a significant amount of processing is still required on the ground. A ground processing system has been designed to generate the higher level products from the satellite data. A structured approach to data handling is required to not allow only accessible storage and analysis of data.

A similar concept of data levels (Level 0–2) used on other satellites has been adopted for the TDS-1 GNSS-R data products in order to help in the definition of processing and data access. A diagram shows the flow in Fig. 13, followed by a discussion of the products below.

1) *Level 0*—Data sampled directly from the RF frontend, which is only stored and downloaded when scheduled. This typically includes raw data from both nadir and zenith antennas, stored as 2-bit In-Phase (no quadrature) data in packet format. Duration from 1–4 min depending on antenna inputs logged.

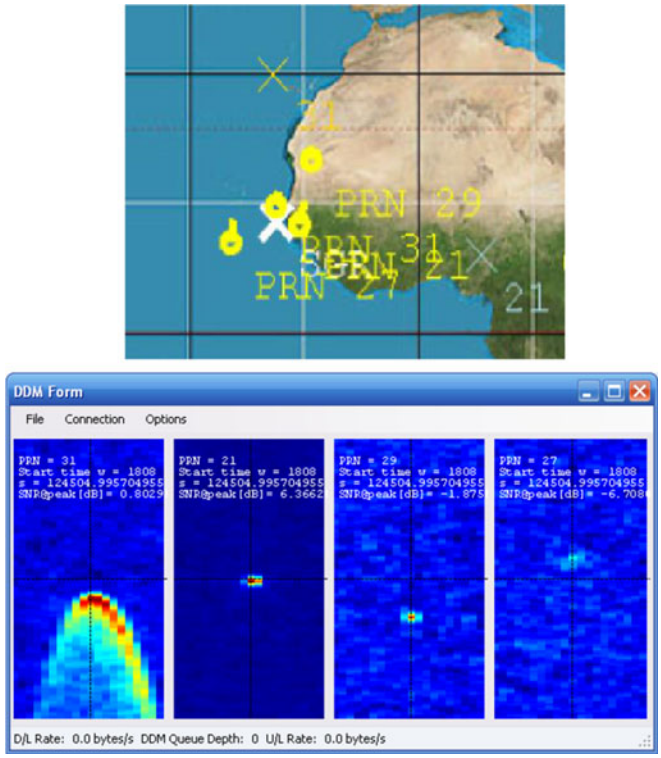

Fig. 12. SGR-ReSI position (white cross) and tracked reflections (yellow circles) at 10:34:49 UTC (PRNs 21, 27, 29 and 31) (b) DDMs generated showing reflections from both ocean and land.

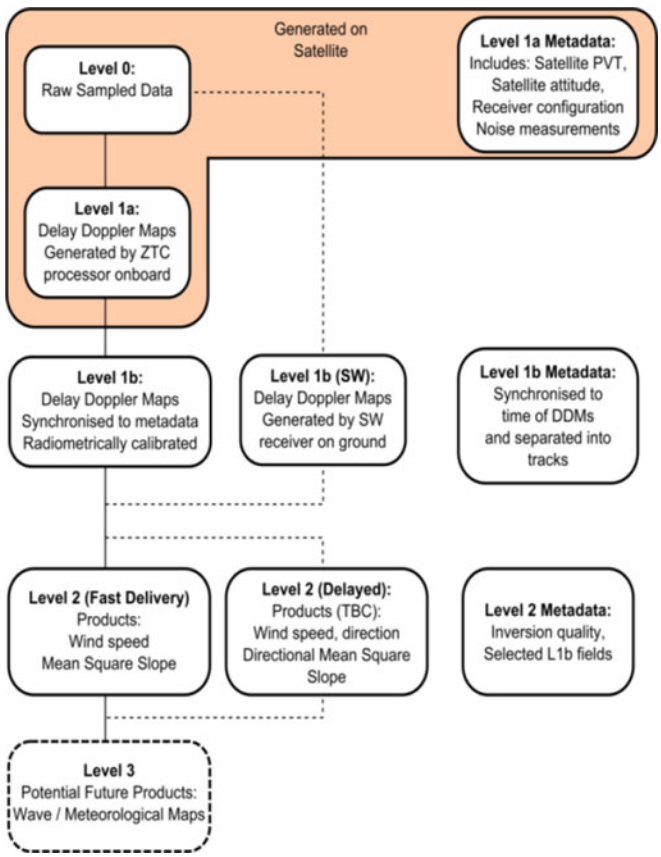

Fig. 13. Wind TDS-1 GNSS-R product levels.

2) *Level 1a*—This contains nadir DDMs processed onboard using ReSI's ZTC unit, nominally 1 DDM per second from four separate reflections. Data is interleaved and may contain measurements during calibration load switching operations. Up to 48 h data over two days, but usually in 2 h chunks.
3) *Level 1b*—This reformats the Level 1a DDMs into TIFF image format, separated into tracks, and is accompanied by detailed xml metadata that synchronizes position velocity and time from the GPS solution, and provides prepared calibration information.
4) *Level 1b(SW)*—Postprocessed using software receiver from L0 collections into a similar format to L1b derived from on-board ZTC processed L1a data. Data length 1–4 min as per L0 data, but may contain more than four reflections per second.
5) *Level 2*—Derived geophysical parameters at same resolution as Level 1 data. Currently, only empirically derived fast delivery products, wind speed, and mean square slope (MSS) are available, but further products are under development.

The **metadata** for the SGR-ReSI is substantial and vitally important for interpretation of the Level 1b DDMs in particular. This includes the location of TDS-1, the GPS satellites, and the specular points (SPs) (as calculated by the ReSI) for each track, the antenna gain, the satellite attitude, and radiometric calibration information.

The payloads on TDS-1 have been allocated a slot in a rolling eight-day cycle, and the SGR-ReSI is operated for two days out of eight. Data from each of these cycles has been grouped, labeled, and numbered according to a "Receiver Data" RD identifier. As a subdivision within the RD number, tracks are sequentially numbered. More details about data and metadata formats are available from the MERRByS Product Manual resources in [10].

B. Constraints of Operation on TDS-1

The TDS-1 mission has been achieved on a limited budget and this extends to the operating regime, with resulting impacts on the data acquisition. Routine data logging from the SGR-ReSI takes place on Days 1 and 2 of the eight-day cycle, while less routine events, such as code uploads and experimentation can only take place on Days 7 and 8. When these days overlap the weekend, plans may be postponed until the next cycle and data collection is put on hold over the Christmas vacation due to limited cover from the Operations Team.

As a part of its technology demonstration, TDS-1 carries a new generation on-board computer (OBC), but initial operations have been using the heritage older generation OBC. One of the limitations of the older OBC is that the data packet rates from the SGR-ReSI are close to its handling limit, and a small proportion of data packets carrying position information from the SGR-ReSI are lost. This means that interpolation has been required to ensure continuity and usability of the metadata. Furthermore, early operations of the ReSI sometimes led to an apparent systematic halt in data logging after a few hours. As a work around, the ReSI has been operated for periods of two orbits, with a refresh cycle over one of the poles.

While new satellite attitude determination and control equipment has been embarked on TDS-1, the baseline attitude performance of the mission was not specified to a high level due to budget constraints, and as none of the demonstrator payloads were deemed to have critical dependence on attitude accuracy. Nominally TDS-1 is controlled with an attitude target of (0, 0, 0)° in an orbit-defined roll, pitch, and yaw, respectively, i.e., Earth pointing. Early operations have shown that the attitude determination and control performance has been adequate for the safety and power levels of the satellite, and for the majority of the technology demonstrations. The attitude performance, however, may prove to impose limitations on the retrieval capabilities and the validation of higher level GNSS-R products such as Level 2 wind speed. In particular, the attitude estimate from TDS-1 is seen to show an excursion of up to 10° when exiting from eclipse conditions into sun light. This suggests that the underdetermined on-board Kalman-filtered attitude estimate drifts from the true attitude while relying solely on magnetometer readings until the more accurate sun sensor suddenly becomes available. The effect of an unknown 10° error in attitude is to give an incorrect antenna gain at the SP (AGSP) which directly impacts the geophysical inversion process. This attitude uncertainty will give smaller errors when reflections are close to the boresight of the antenna, where the antenna gain changes slowly in azimuth and incidence, but will result in large errors when reflections are outside the main antenna lobe where the gain can change rapidly with azimuth and incidence angle.

C. Instrument Gain Settings and Observables

Similarly to the UK-DMC experiment, the RF frontends used in the SGR-ReSI are commercial off-the-shelf parts intended for terrestrial GPS/GNSS applications. Under normal operation, received GNSS signals prior to correlation are below ambient noise, and the frontend RF gain adjusts to accommodate the potentially varying ambient noise level using automatic gain control (AGC). Unlike on UK-DMC, the RF frontends in the SGR-ReSI as an alternative can be programed with a fixed gain. For simplicity, initial operations of the SGR-ReSI have been conducted in the AGC mode of operation, both nadir and zenith frontends, referred to as automatic gain mode (AGM). Later operations have made use of programed fixed gain settings, referred to as programmable gain mode (PGM), initially in the nadir channel only.

In AGM, the reflected signal level is subject to unmonitored RF gain changes, and so it is inadvisable to take absolute signal level measurements from the DDM. Instead observables based upon the signal to the noise ratio (SNR) can be formulated, and as the RF gain amplifies both signal and noise, the ratio cancels gain effects out. The noise is used as a reference from which to measure the signal level, so it is dependent on a stable noise floor. There are several ways that SNR observables can be formulated from DDMs; one approach for finding the peak SNR is discussed here. The peak value of a single DDM in the central (0 Hz) Doppler column may be used, and divided by a measure

of the noise from the DDM. The noise value can be taken from the first row of the DDM (a delay with no reflections due to being above the predicted Earth surface) and central Doppler column, or from a box of multiple pixels to improve the noise estimate. A single pixel if correctly selected can be less susceptible to nonaligned autocorrelation products from the GPS code.

Sometimes an offset of (–1) has been applied on the basis that the DDM peak contains not only the signal but an additive noise component as well, though this only becomes significant at low SNRs, and as the noise at one pixel is different to another, it can result in a negative number, causing difficulties in representing the observable in the log domain.

In PGM, the now suboptimal bit distribution will cause the quantization noise to increase. An SNR observable can still be used, but now a direct measure of the signal can be taken, the signal minus noise observable is calculated in a similar way to the SNR observable, though with the subtraction rather than division of noise. This observable is proportional to the received signal power, but has a dependence on a stable system gain. The switched loads in the LNAs can be used to help measure and bound any drift in the gain over time.

One characteristic of the GNSS signals is the cross- and nonaligned autocorrelation peaks caused by the finite length of navigation codes. These could show up in the DDM noise and potentially act as a confounding factor when trying to establish noise levels. There are further discussions of signal radiometric measurement details in [12].

D. Progress in Data Gathering

Level 1a DDM data collection commenced slowly in 2014 with only hours of data at a time, but as the operations were refined, the amount of data collected has increased toward the maximum of 48 h with scheduled refresh cycles over one of the poles. Fig. 14 shows an example of 20 h of data collected over the globe in October. A decimated summary sequence of the DDMs in one track is also shown (this summary process selects 30 evenly spaced DDMs from the track). This illustrates how the signal becomes stronger as it passes through the maximum of the SGR-ReSI nadir antenna gain, before weakening again.

The vertical axis in Fig. 14 also shows a bias present in the on-board estimation of the SP location that was corrected in a code upload on 6th March 2015 (the estimated location is made available from the receiver). SSTL and NOC worked together extensively during the commissioning phase to detect, identify and address bugs and anomalies, and gradually improve the products and metadata.

From the period of September 2014 to April 2015, a total of 5 740 000 valid DDMs were collected, and in one 48 h period alone, 630 000 DDMs can be gathered, when acquiring almost four DDMs/s. This compares with the total of some 5000 DDMs recovered during the entire life of UK-DMC. Fig. 15 shows the availability and increase in data volume over time between September 2014 and February 2015. Fig. 16 shows the geographical distribution of the TDS-1 data acquired over nonland surfaces up to March 2015.

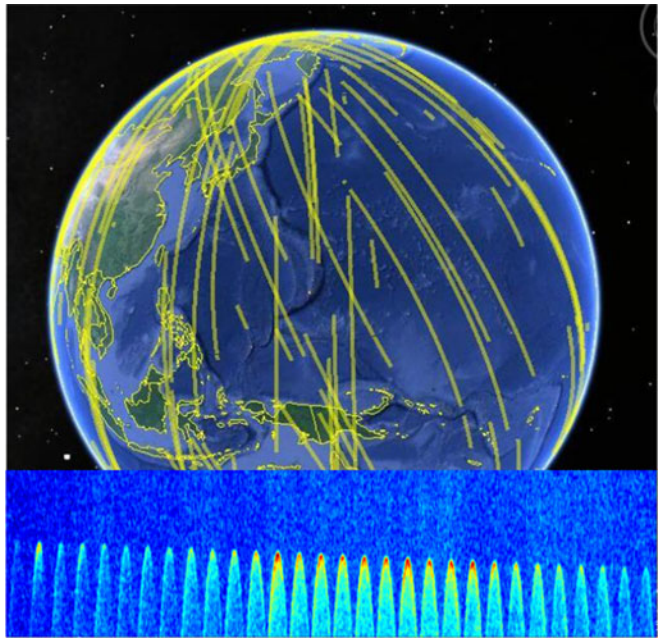

Fig. 14. Example TDS-1 DDM data collection: RD6, 30th October 2014—global coverage and summary of one DDM track.

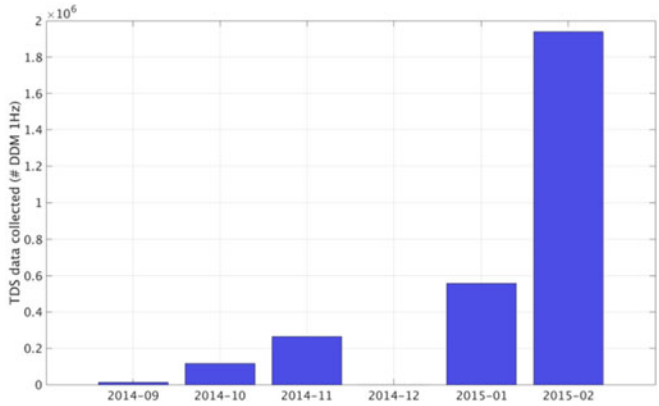

Fig. 15. TDS-1 GNSS-R data acquisition in September 2014–February 2015 shown as number of 1 Hz DDM collected.

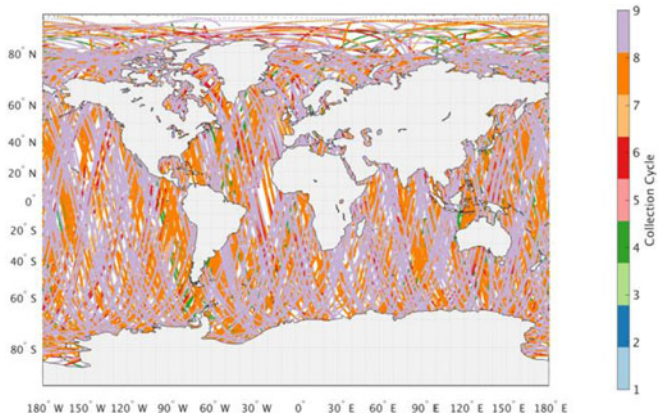

Fig. 16. TDS-1 GNSS-R geographical distribution and coverage from September 2014 to February 2015. For illustration purposes, GNSS-R data acquired over land is not shown.

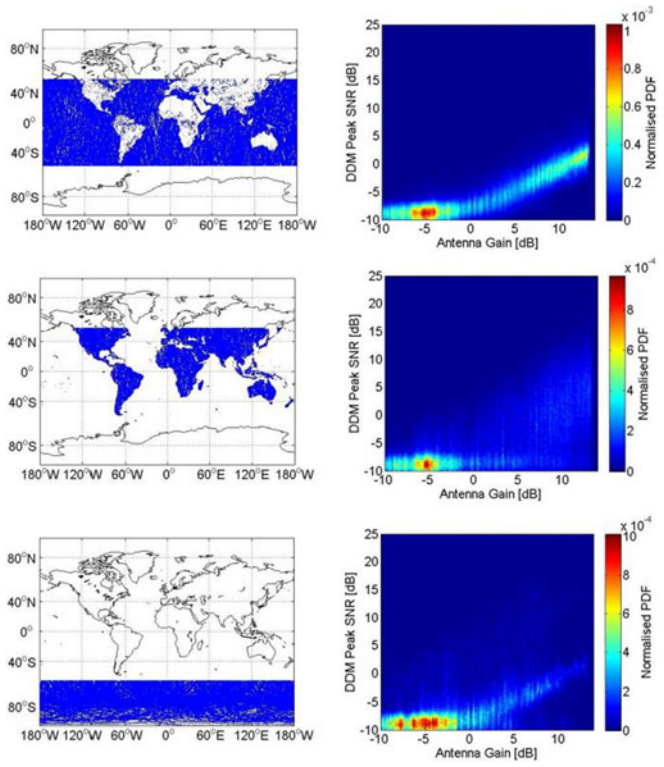

Fig. 17. SNR and antenna gain histogram for SPs (a) Over oceanic regions, (b) over land, (c) over polar regions.

All Level 1a data collected up to 18th April 2015 correspond to the instrument operating in AGM, while later dates have operated in PGM.

In addition to the Level 1 data, Level 0 raw collections continue to be scheduled, typically at a rate of three collections per eight-day cycle. Each Level 0 raw data collection is around 2 min, so around 80 min of raw collections were taken from September 2014 to April 2015. This compares with around 23 min of raw data collected from UK-DMC. The collections have been scheduled in areas of interest and where validation data is available, for example, close to wave buoy locations around Hawaii. Several collections have been scheduled over land and over ice/water transitions and other areas of interest.

E. Data Characteristics

The peak SNR observables of a large quantity of the Level 1 data were computed and categorized into three regions: ocean, land, and polar, where 55° latitude was used as the threshold to separate ice-free ocean from polar regions (see Fig. 17). In this example, only data from the Antarctic region is shown to represent polar regions.

When the peak SNR observable is plotted against antenna gain, a series of observations can be made. At the lowest antenna gain in each plot, the detectability limit is visible as a cloud of points at below –7 dB SNR. This is the population where the reflection signal power, in combination with the antenna gain is insufficient for the signal to be detectable above the thermal noise. By considering a column of constant antenna gain, where the SNR is higher than this thermal noise, the distribution of SNR will correspond to the distribution of reflected power.

The ocean reflections exhibit a range of around 15 dB in SNR for constant antenna gain, with most of the data within a range of 5 dB. The land reflections exhibit a greater than 25 dB range in SNR for constant antenna gain. The DDMs over the Antarctic show multiple discrete populations. This is representative of the wide range of surface types that will be included in this surface selection set, including and not limited to, very smooth surface sea ice, very rough land ice reflections, and ocean reflections. For Antarctica, the frequency of low antenna gain DDMs shows the limited number of reflections within the beamwidth at this latitude. The reflectometry antenna is near-nadir pointing, so picks up strongest reflections from the transmitters near zenith. However, with the GPS constellation at 55° inclination, no nadir reflections will be present close to Earth's poles.

The characteristics of the data from TDS-1 also give indications for the potential for other products. Most notably, when a reflection track crosses from ocean to sea ice, there is a clear change in the peak SNR, suggesting the practical possibility of an ice-edge detection metric.

VI. Ocean Inversion and Validation Activities

Previous work using data from UK-DMC over the ocean had established the basis for Level 2 inversion algorithms for wind speed and MSS [2], [3] based on SNR and these formed the foundation of the preliminary analyses of TDS-1 data for wind retrieval.

A. GNSS-R Level 2 Wind Speed Inversion Algorithms

So far, two types of Level 2 wind speed inversion algorithms have been investigated at NOC for TDS-1: the so-called "fast-delivery inversion" algorithm (FDI) and the more complex "bistatic radar equation" algorithm (BRE). Both algorithms are based on the SNR calculated here as the ratio of the average signal power (S) in a box located around the peak of the DDM and the average noise power (N) measured in a noise box in the signal-free area (see Fig. 18), i.e., SNR $= S/N$.

For both algorithms, the size of the signal box is chosen to achieve a spatial resolution around 25 km. For TDS-1, the dimensions of the signal box are 1 chip (four delay bins) by 1500 Hz (three Doppler bins) corresponding to a spatial resolution between 22 and 30 km (median value 25 km) depending on the elevation angle of the SP. Since the position of the peak can fluctuate in both delay and Doppler space, the signal box is positioned dynamically around the peak using an automatic peak detection scheme based on the application of a median filter and extraction of the local maxima in the DDM.

The BRE algorithm is a detailed inversion model that corrects for the GNSS-R bistatic viewing geometry and the receiver antenna gain pattern effects in accordance with the GNSS-R BRE. It is based on work by Gleason [8], which is in turn based on the theoretical model by Zavorotny & Voronovich [13]. A full description of the BRE algorithm and its performance can be found in [14]. Briefly, Foti *et al.* [14] showed that, for SNR $>$ 3 dB, TDS-1 BRE wind speeds are retrieved without

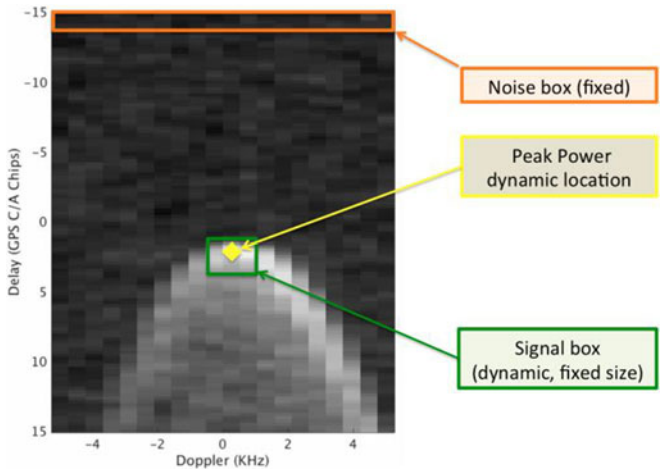

Fig. 18. Calculation of the GNSS-R SNR for a TDS-1 SGR-ReSI delay-Doppler Map.

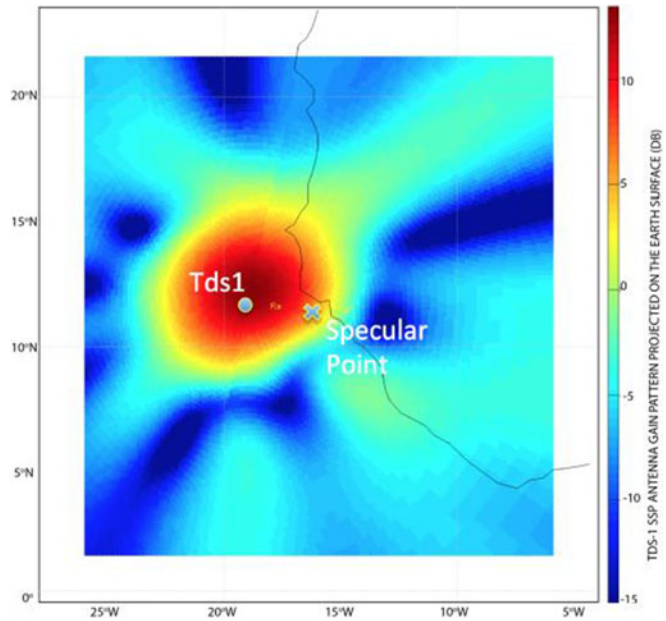

Fig. 19. Zoomed view of the TDS-1 nadir antenna gain pattern (dB) projected on the Earth surface (here shown off the west coast of Senegal).

bias and with a precision around 2.2 m/s for winds between 3-18 m/s, even without calibration. Its drawback is that BRE is not simple to implement in the MERRByS ground-processing system, and its processing speed makes it less suitable for a rapid data delivery.

By contrast, the FDI algorithm is a simple empirical inversion developed from spaceborne GNSS-R measurements acquired with TDS-1, and designed to allow rapid inversion. The only essential inputs to FDI are the SNR from the Level 1 DDMs and the AGSP. The FDI was implemented for the MERRByS portal to swiftly deliver TDS-1 Level 2 wind speed products in a simple easy-to-understand format to engage potential operational end users of the data.

B. Collocation With METOP ASCAT A/B

The BRE and FDI algorithms were developed and validated with a globally distributed matchup dataset of TDS-1 GPS-R data collocated with a surface wind speed from the METOP ASCAT-A/B satellite scatterometers. It turned out that the TDS-1 injection orbit was particularly favorable to collocations with the METOP-A and METOP-B satellites. This provided the convenient means of gathering large quantities of GNSS-R data at the beginning of the TDS-1 mission collocated with established independent wind estimates for verification purposes. We note that, with time, the opportunity to collocate TDS-1 with METOP-A/B reduces in view of the TDS-1 LTAN drift.

The ASCAT data were taken from the ASCAT Level-2 25 km Swath products available through PO.DAAC (https://podaac.jpl.nasa.gov/). ASCAT data were collocated within 1 h and 1° of latitude/longitude of TDS-1 and correspond to 10 m wind speed over ice-free and rain-free ocean conditions. ASCAT data quality control (QC) was based on the application of all data quality flags provided in the L2 25 Km swath products, so that only ASCAT data that passed all QC checks were retained (including flags for rain, ice, land, mispointing, etc.). Due to the favorable orbital elements of TDS-1 at the beginning of the mission, it was found that over 67% of TDS-1 data could be successfully collocated with the METOP constellation within 1 h/1°. A spatially uniform global distribution is observed, covering wind speeds typically up to 15 m/s but with one incidence of a maximum of 27.9 m/s. This value was reported by ASCAT-B in the Southern Ocean on 31 October 2014 [14]. Note that by its nature, ASCAT only permits the validation of the Level TDS-1 Level 2 wind speed, and not MSS Level 2 product.

C. NOC-FDI Development and Performance

The TDS-1/ASCAT matchup dataset served to establish the empirical relationship between SNR, surface wind speed, and the AGSP. The AGSP has a dominant effect on the SNR and needs to be accounted for using knowledge of the position of the SP on the surface within the antenna gain pattern. Fig. 19 shows a zoom of the TDS-1 sea-state payload antenna gain pattern projected on the Earth surface, indicating the highly directional main beam (pointing approximately 6° behind the satellite). Note the very significant changes in AGSP over short distances immediately outside the main antenna beam. SNR from SP in those areas will be highly sensitive to satellite attitude uncertainty, which will introduce large errors in the knowledge of the AGSP and, therefore, the retrieved wind information.

The TDS-1 SNR measurements are compared with ASCAT U10 in Fig. 20, and manifestly display a power-law relation stratified by AGSP.

This dataset includes all reflections with AGSP greater than 0 dB for which a signal could successfully be estimated (see calculation of SNR in Section VI-A) and, therefore, includes samples located far away from the main lobe of the antenna. The behavior is similar to what had been suggested by the UK-DMC GNSS-R ocean data collocated with WindSat winds (albeit with

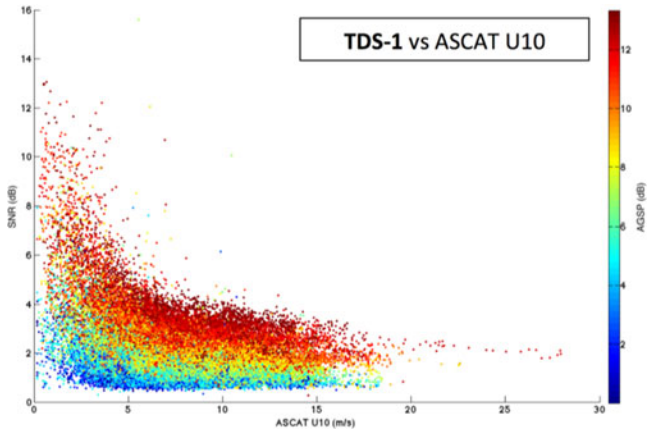

Fig. 20. Relationship between ASCAT U10 and TDS-1 GNSS-R SNR (dB).

a much smaller number of samples) and by simulated data from the CYGNSS end-to-end simulator [15].

The empirical relation can be approximated by a power law with fitted coefficients determined by least-square fitting of the TDS-1 data as

$$\mathrm{U10} = \mathrm{AX\hat{}B} \tag{1}$$

with X = SNR - k1 ∗ AGSP + k2. For TDS-1 data acquired in AGC mode (i.e., all data up to March 2015), the nominal values of A, B, k1, and k2 for TDS-1 are 97.24, –2.28, 0.215, and 3, respectively.

The FDI relation and the retrieved winds obtained for the matchup dataset are shown in the subplots in Fig. 21. The general performance of the FDI algorithm achieves a bias around 0.2 m/s and a root-mean-square error just below 4 m/s. Although this performance may seem poor, one must remember that no correction was applied for differences in geometry and that all SP are included in this analysis, including many that occur for very low values of AGSP where signal strength is low and uncertainty on AGSP is large.

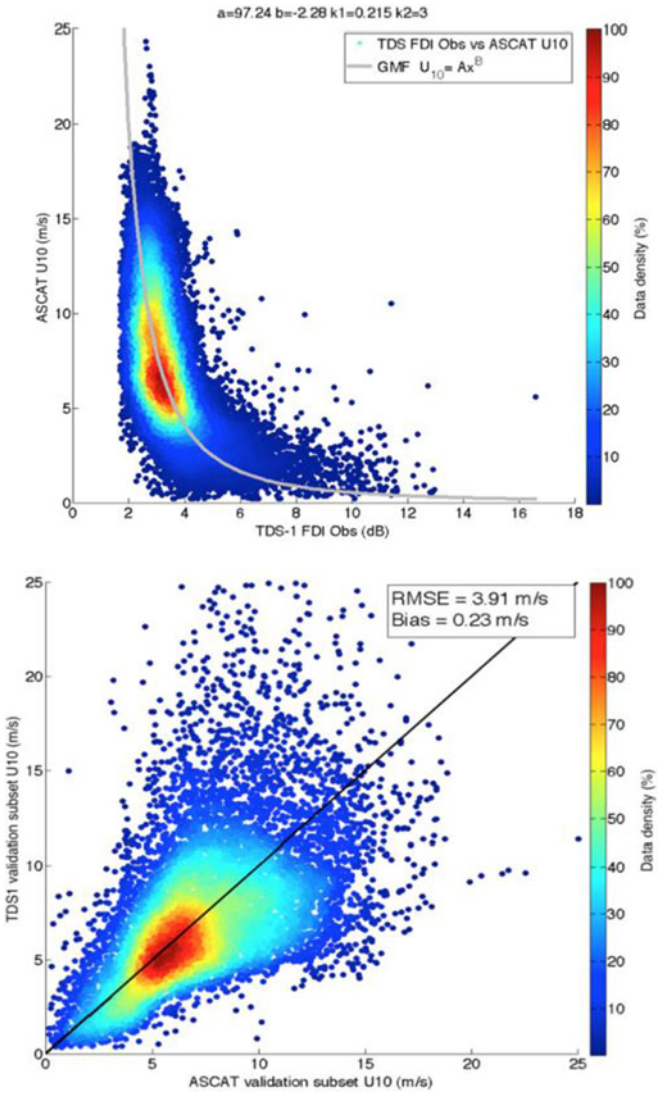

Fig. 21. TDS-1 FDI: top) Two-dimensional histogram of the randomly selected subset of TDS-1/ASCAT matchup data used for least-square fitting (75%) and the fitted empirical power law relating U10 to SNR; bottom) Retrieved TDS-1 wind speed against ASCAT winds for the remaining independent validation subset (25%) of the TDS-1/ASCAT matchup database.

D. NOC-FDI Level 2 Wind Speed Products on MERRByS

The NOC-FDI Level 2 algorithm was implemented in the MERRByS ground processing system to routinely produce and distribute Level 2 wind speed products to potential end users. Unfortunately, the first implementation of the Level 2 FDI algorithm featured a software bug, which resulted in invalid Level 2 FDI wind products being produced and disseminated for some time via the MERRByS web portal. Invalid TDS-1 Level 2 winds are characterized by unrealistically high biases of up to 6 m/s.

For practical reasons, this issue could not be resolved until recently, but software correction and reprocessing have now been implemented. Following successful revalidation by NOC of the output of the operational ground processor (see Fig. 22), new L2 wind products (Version 1.11) are now available on MERRByS for the full period September 2014–February 2015. Note that revalidation in Fig. 22 show results for the full dataset up to February 2015, while those shown in the bottom subplot in Fig. 21 represent a much smaller subset of the available data.

E. Further Investigations of GNSS-R Signals Over Ocean

The availability of large quantities of GNSS-R measurements is now enabling new investigations into the behavior of GNSS-R signals. Together with theoretical models and numerical end-to-end GNSS-R simulators, these data will help over the next few years to answer important long-standing questions about the dependence of GNSS-R signals on various instrument, geometrical, and geophysical parameters. Improved attribution of the variability seen in GNSS-R signals will be essential in order to get a handle on instrument and GNSS-related effects and to better prepare for future GNSS-R missions such as CYGNSS and GEROS on the International Space Station.

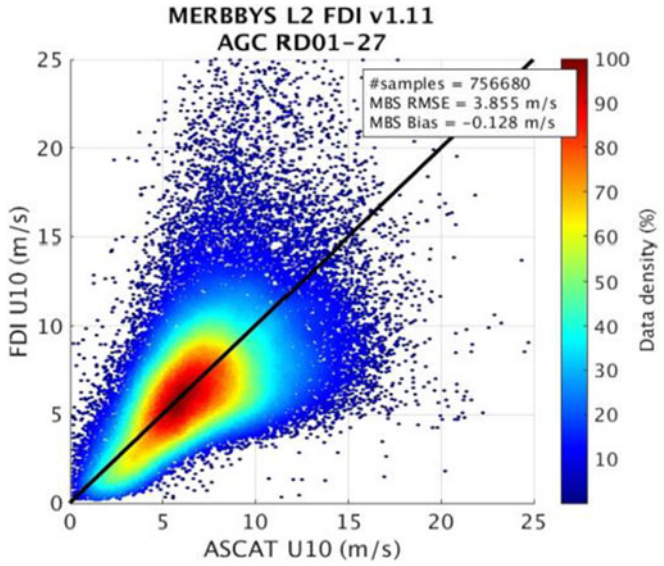

Fig. 22. Revalidation of the Level 2 FDI wind speed products (Version 1.11) now available on MERRByS.

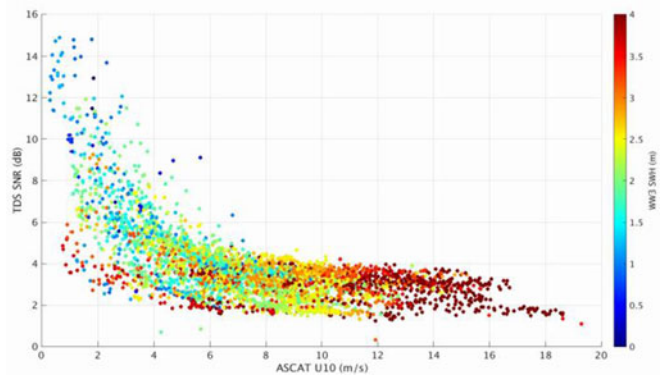

Fig. 23. TDS-1 SNR (dB) versus ASCAT U10 (m/s) for TDS-1 data limited to samples where AGSP $>$ 13.1 dB. Colours show the collocated significant wave height (m) from the Ifremer WaveWatch3 numerical ocean surface wave model [18].

The possible secondary sensitivity of GNSS-R signals to sea state has long been mooted, mainly because of the known dependence on sea state observed in specular reflections at nadir in satellite altimetry [16], [17]. Here, Fig. 23 presents empirical evidence that geophysical effects linked to sea state are indeed present in spaceborne GNSS-R measurements over the ocean. The figure shows SNR against ASCAT U10 for TDS-1 data acquired with AGSP greater than 13.1 dB, with colors indicating Significant Wave Height at the time and location of the TDS-1 SP obtained from the WaveWatch3 numerical ocean surface wave model [18]. Limiting the data to high AGSP values focuses the analysis on an SP collected near the main peak of the antenna gain, thereby reduces signal variability linked to antenna gain uncertainty caused in turn by platform attitude errors. Fig. 23 shows the clear effect of sea state on SNR at low wind speed below 6 m/s. Thus, nonlocal wave effects contribute to roughening the ocean surface and reduce SNR. In these cases, application

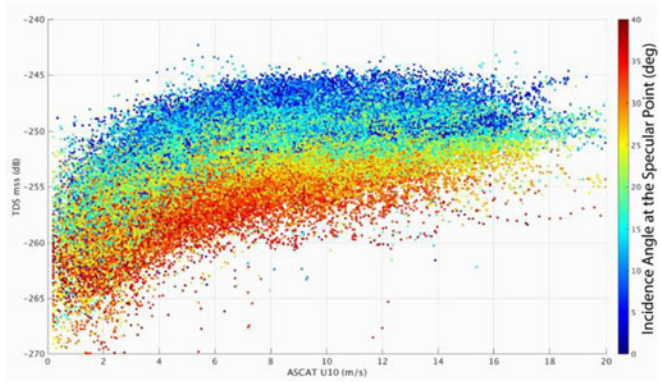

Fig. 24. TDS-1 MSS versus ASCAT U10 with colors indicating incidence angle at the SP (0°= nadir). MSS is calculated as $1/\sigma 0$ and shows clear stratification with incidence angle even after correction for AGSP and bistatic geometry.

of a standard wind speed inversion algorithm that does not account for sea state would result in overestimated wind speeds. Unfortunately, the TDS-1 dataset remains presently too sparse to determine whether sea-state effects also exist at moderate and high winds, or to investigate mitigating strategies.

Similarly, Fig. 24 shows the first experimental confirmation of the residual dependence of the GNSS-R bistatic radar cross section on incidence angle at SP. In this figure, TDS-1 data shown are the MSS, which is computed as the inverse of the bistatic radar cross section, $\sigma 0$. Thus, even after correcting for antenna gain, transmitter range, receiver range, and changes in the size of the glistening zone, the GNSS-R $\sigma 0$ shows a very clear stratification with incidence angle. If appropriate, this effect could be easily estimated and accounted for in wind inversion algorithms to extend the applicability of the algorithms to SP collected in all parts of the antenna beam.

VII. Collections Over Land

It can be noticed in Fig. 17 that the reflected signal to noise has an extremely large dynamic range over land. When the peak signal to noise of each DDM is plotted over a map, it become apparent that there are regions on the ground where reflections are consistently weak, and other areas where they are consistently strong, suggesting that the measurements may contain a valuable geophysical information.

Two examples of this are given in Fig. 25 from the Amazon basin and Australia.

As expected, healthy rainforests such as in the Amazon are good absorbers of electromagnetic radiation, primarily in the visible spectrum but also at lower frequencies. It is also known that mirror-calm surfaces, such as rivers and lakes are likely to give very strong reflections. Over the Amazon, this contrast between forest and rivers is clearly visible. The contrasts over Australia are perhaps more surprizing, as there is less in the way of rain forests and rivers, yet there are strong variations in reflection strength with a clear geophysical imprint visible. Variations may be due to soil moisture, vegetation, surface roughness, and surface salinity.

As with the measurements over the ocean, further work is expected that could offer improvements to the retrievals in terms of

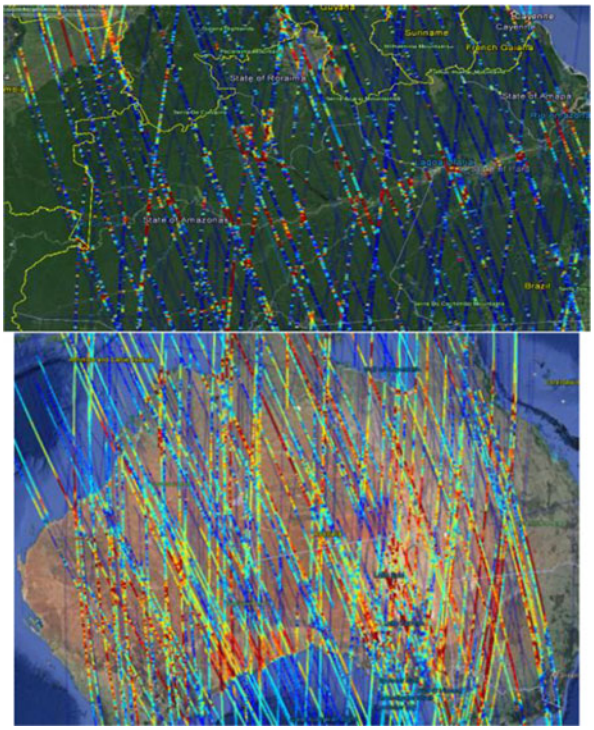

Fig. 25. Reflected SNR over (a) the amazon basin (b) Australia. Blue tracks indicates weak reflections, red indicates strong reflections.

data filtering and calibration. Measurements over the land have some special considerations too, for example, reflections off high mountains will be lost from the DDMs unless the elevation is allowed for within the reflection predictions. Changes in measurements over time may contain the most useful hydrological and biomass information.

VIII. Collections Over ICE

With regular measurements being taken over polar regions, TDS-1 provides a clear opportunity to develop the cryospheric applications of GNSS-R. For the first time, a large dataset of spaceborne GNSS-R data is available for validation of ice monitoring algorithms. There appears to be a strong contrast between ocean and ice reflections allowing for edge and ridge detection algorithms to be implemented over a track with filters and techniques similar to those in [19]. An example implementation of such a method is shown in Fig. 26 illustrating potential applications for an ice-edge detection. If the limitation is assumed to be due to the iso-delay ellipse of the C/A code, then a resolution of 7–14 km is anticipated. The strength of the reflections off ice could in future enable GNSS-R altimetric measurements without the need for a higher gain antenna than is used on TDS-1.

IX. On-Going Activities

A. Data Access

Much of the data from TechDemoSat-1 GNSS-R experiment has been made available at the MERRByS website [8]. The data has been released under a Creative Commons Licence that allows free access for noncommercial use.

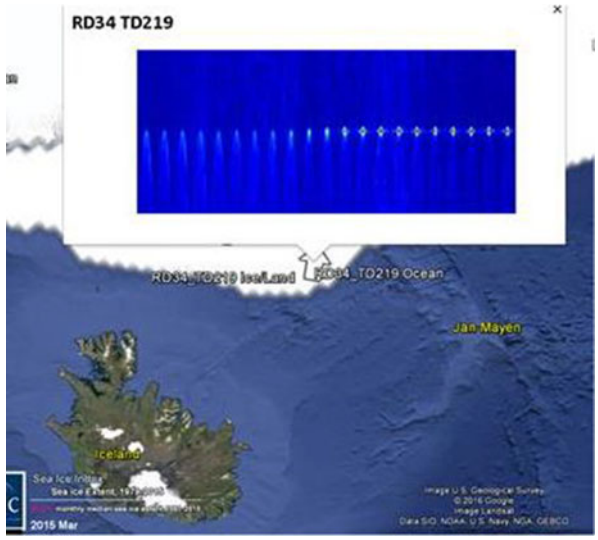

Fig. 26. Sequence of DDMs over a sea/ice boundary near Iceland, March 2015. The white arrow indicates the boundary as detected by Canny edge detection routine.

A small number of example datasets are provided at Levels 0, 1, and 2 without requiring a log-in. When users have a password, they have access to a large collection of Level 1b and Level 2 data for the TechDemoSat-1 mission.

A map-based interface makes it possible to search for tracks, and view quick look information. A summary of each search is created in KML, such that it can be viewed in Google Earth with the ability to graphically view parameters signal to noise and antenna gain.

From this, users are able to navigate through each track and observe directly the correspondence of the SNR with the geophysical features on the ground.

On 5th March 2015, NOC and SSTL hosted a TDS-1 User Consultation Workshop where first results from TechDemoSat-1 GNSS Reflectometry Experiment were presented. The meeting saw enthusiastic participation from national and international delegates representing a broad spectrum of interests from academia, operational weather forecasting institutions, space agencies, and commercial providers of downstream services. Presentations were streamed live over the web for interested parties in the US and continental Europe who were unable to attend. At this event, access to the MERRByS Website was made available through allocation of user passwords. Furthermore, users were notified at the GNSS Reflectometry workshop in Potsdam, May 2015 (GNSS+R 2015 [20]), which features early results with TechDemoSat-1 data by several groups.

B. Further Work

A follow-on study called "TDS-1 Exploitation Campaign for Future Sea State Monitoring" with SSTL and NOC and support from ESA will continue the work with the TechDemoSat-1 SGR-ReSI. The areas of interest include the following.

1) Data Collection: Data will continue to be collected on a regular basis. Depending on mission constraints, longer periods of data may be collected, i.e., for more than two days within the

TDS-1 eight day cycle. Raw data will also be collected over areas of interest, and where possible, over high winds and calibration targets. Some minor anomalies and configuration issues in the SGR-ReSI still occasionally cause data outages, so these will be addressed.

2) Instrument Calibration Activities: The fixed gain and switched load capabilities of the SGR-ReSI are to be fully enabled. This would mitigate variations in noise that are significant but currently unaccounted for. Further calibration information is available from the direct signals. The attitude knowledge of TDS-1 is a limiting factor on retrievals, especially away from the antenna boresight, but there are measures that can be taken to achieve improvements. There are three experimental sensors on TDS-1 that could potentially be employed to better attitude knowledge, and improve L2 retrieval coverage. External campaigns may permit the verification of the calibration.

3) Processing Investigation: A number of processing parameters can be tuned on TDS-1 which could affect the quality of data collection and L2 retrievals, such as coherent integration time, resolution of Delay and Doppler, etc. By experimenting with raw data, and testing options in orbit, an attempt to find optimal settings will be undertaken.

4) Ground Processing: The ground processing needs to be expanded to handle new calibration metadata, such as switched loads, direct signals, with resultant documentation. Improvements can be brought into MERRByS that have been requested by users. The low-operating duty cycle and limited ground station support will never permit near-real time data service with TDS-1, but some of the elements can be demonstrated, such as rapid data processing and dissemination.

5) GMFs and Validation: Once the calibration system has improved, it is expected that the fitting and validation of NOC-FDI and BRE algorithms will achieve better results. The MSS is being retrieved but has not yet had any validation.

6) Advanced Experimentation: There are advanced hardware capabilities on TechDemoSat-1 that have not yet been commissioned. The capability of picking up dual-frequency reflections could open up new applications, especially for altimetry over ice. The hardware is capable of collecting reflected Galileo signals but these have not been targeted yet—the wider bandwidth could improve the resolution of measurements taken on the ground.

7) Science Study: A further study called "Scientific Assessment of TDS-1 GNSS Scatterometric Measurements" is planned by ESA that would undertake a scientific assessment of the TDS-1 GNSS-R data. This will be looking in more detail at a model-based retrieval, i.e., a delayed mode product. As well as improving understanding and perhaps applicability of retrieval accuracy, this could help derive new but equally valuable products such as wind direction.

C. CYGNSS Mission

Beyond TechDemoSat-1, the SGR-ReSI receiver will be flying (current launch in 4Q-2016) as the primary payload on CYGNSS constellation, funded under NASA's Earth Venture 2 programe [3]. This eight nano-satellite constellation is primed by the University of Michigan and being constructed by Southwest Research Institute. Its target application is to take wind speed measurements within hurricanes, helping to save lives though improvements to forecasting and monitoring. Many of the results and lessons learnt from TDS-1 will help prepare for the CYGNSS mission. The large quantity of data expected will achieve a new level of coverage compared to TDS-1.

X. Conclusion

This paper has presented an overview of the GNSS-Reflectometry experiment on the UK TechDemoSat-1 (TDS-1) mission. The motivation for the development of the instrument came from an initial experiment on the UK-DMC mission in 2003, and led to an instrument that is able to process measurements on-board into DDMs. The satellite was launched in July 2014, and since then data has been gathered both in the form of DDMs and also unprocessed data collections. Preliminary work has been done on inverting the measurements into Level 2 products, specifically wind speed and mean-squared slope over the ocean, with promising results. Reflections recovered over the land surface are also showing a strong geophysical imprint, suggesting potential for hydrological and vegetation related retrieval.

Both ocean and land applications will benefit from further characterization of the measurements and calibration improvement activities. Clearly, a single satellite is inadequate for addressing the temporal resolution required for effective sea-state measurement, or even for observing seasonal changes in hydrological cycles over the land. The CYGNSS mission will be the first to make use of the low size weight and power of GNSS Reflectometry instruments, as an enabler for a constellation of eight satellites. Even so, this will only be targeting the globe at inclinations lower than 35° inclination, and the full benefits will only be achievable when there is a larger constellation that is able to cover the higher as well as lower latitudes.

Acknowledgment

The authors would like to acknowledge contributions from other members of SSTL staff, and from T. Peterken, placed in SSTL under the SATRO scheme.

References

[1] M. Unwin, S. Gleason, and M. Brennan, "The space GPS reflectometry experiment on the UK disaster monitoring constellation satellite," in *Proc. ION GPS 2003*, Portland, OR, USA, Sep. 2003, pp. 2656–2663.

[2] S. Gleason *et al.*, "Detection and processing bistatically reflected GPS signals from low earth orbit for the purposes of ocean remove sensing," *IEEE Trans. Geosci. Remote Sens.*, vol 43, no. 6, pp. 1229–1241, Jun. 2005.

[3] M. P. Clarizia, C. P. Gommenginger, S. T. Gleason, M. A. Srokosz, C. Galdi, and M. Di Bisceglie, "Analysis of GNSS-R delay-doppler maps from the UK-DMC satellite over the ocean," *Geophys. Res. Lett.,* vol. 36, no. 2, 2009, Art. no. L02608.

[4] C. Ruf *et al.*, "CYGNSS: Enabling the future of hurricane prediction," *IEEE Geosci. Remote Sens. Mag.*, vol. 1, no. 2, pp. 52–67, Jun. 2013, doi: 10.1109/MGRS.2013.2260911

[5] ESA SP-1329 EO Science Strategy for ESA, Feb. 2015, [Online]. Available: www.esa.int

[6] CEOS DRM Observation Strategy, 2013, [Online]. Available: www.ceos.org

[7] P. Jales, "Spaceborne receiver design for scatterometric GNSS reflectometry," Ph.D. dissertation, Surrey Space Centre, Univ. of Surrey, Surrey, U.K., 2012.
[8] S. Gleason, "Remote sensing of ocean, ice and land surfaces using bistatically scattered GNSS signals from low earth orbit," Ph.D. dissertation, Univ. of Surrey, Surrey, U.K., 2006.
[9] M. Unwin, S. Duncan, P. Jales, P. Blunt, and J. Tye, "Implementing GNSS-reflectometry in space on the TechDemoSat-1 mission," in *Proc. ION GNSS*, Tampa, FL, USA, Sep. 2014, pp. 1222–1235.
[10] www.merrbys.org Mission and Product Descriptions, May 2016, [Online]. Available: http://www.merrbys.co.uk/Resources%20Page.htm
[11] Celestrak, Source of Two Line Elements, May 2016, [Online]. Available:www.celestrak.com
[12] J. Tye, P. Jales, M. Unwin, and C. Underwood, "The first application of stare processing to retrieve mean square slope using the SGR-ReSI GNSS-R experiment on TDS-1," *IEEE J. Sel. Topics Appl. Earth Observ. Remote Sens.*, 2016, doi:10.1109/JSTARS.2016.2542348
[13] V. Zavorotny and A. Voronovich, "Scattering of GPS signals from the ocean with wind remote sensing application," *IEEE Trans. Geosci. Remote Sens.*, vol. 38, no. 2, pp. 951–964, Mar. 2000.
[14] G. Foti *et al.* "Spaceborne GNSS-reflectometry for ocean winds: First results from the UK TechDemoSat-1 mission," *Geophys. Res. Lett.*, vol. 42 no. 13, pp. 5435–5441, Jul. 2015, doi:10.1002/2015GL064204
[15] C. Ruf, "private communication," Jan. 2014.
[16] C. Gommenginger, M. Srokosz, P. Challenor, and P. Cotton, "Development and validation of altimeter wind speed algorithms using an extended collocated buoy/Topex dataset," *IEEE Trans. Geosci. Remote Sens.*, vol. 40, no. 2, pp. 251–260, Feb. 2002.
[17] C. Gommenginger, M. Srokosz, P. Challenor, and P. Cotton, "Measuring ocean wave period with satellite altimeters: A simple empirical model," *Geophys. Res. Lett.*, vol. 30, no. 22, 2003, Art. no. 2150, doi:10.1029/2003GL017743
[18] IOWAGA Integrated Ocean Waves for Geophysical and Other Applications, May 2016, [Online]. Available: http://wwz.ifremer.fr/iowaga
[19] J. Canny, "A computational approach to edge detection," *IEEE Trans. Pattern Anal. Mach. Intell.*, vol. PAMI- 8, no. 6, pp. 679–698, Nov. 1986.
[20] GNSS+R 2015 Workshop, Potsdam, May 2015, [Online]. Available: www.gnssr2015.org

Martin Unwin received the Ph.D. degree in the subject of spaceborne GPS from the University of Surrey, Guildford, U.K. during 1991–1995.

He initiated and led the GPS team in SSTL, designing the SGR-20 space GPS receiver, which flew on UoSAT-12 and Proba-1. The GPS team succeeded in demonstrating autonomous orbit control, attitude determination in orbit, operation of GPS above the GPS constellation, and the feasibility of GPS reflectometry on the UK-DMC satellite. He has had involvement in GIOVE-A and Galileo FOC projects from the beginning. He is currently a Principal Engineer in SSTL and is working on the development of the SGR-Axio receiver, the SGR-ReSI exploitation on TechDemoSat-1, and the NASA CYGNSS mission.

Dr. Unwin won the Institute of Navigation Tycho Brahe Award 2011 and the GPS World Leadership Award 2012.

Philip Jales received the M.Phys. degree in physics from the University of Manchester, Manchester, U.K., in 2007. He received the Ph.D. degree from the University of Surrey, Guildford, U.K., in 2012, on the topic of GNSS-reflectometry techniques, specializing in new receiver approaches.

He is currently a Senior Engineer at SSTL working on the reflectometry-capable space GNSS receivers, the SGR-ReSI, and SGR-Axio. He is supporting both the NASA CYGNSS mission and the TechDemoSat-1 reflectometry exploitation experiment.

Jason Tye received the M.Sci. degree in theoretical physics from the University of Birmingham, Birmingham, U.K., in 2013. Since then, he has been working toward the Ph.D. degree on developing the applications of spaceborne GNSS-R, utilizing data from SSTL's SGR-ReSI on TechDemoSat-1 at the University of Surrey.

His research interests include understanding receiver effects on delay-Doppler maps and novel methods of wave and ice sensing.

Christine Gommenginger received the Diplome d'Etudes Approfondies degree in electromagnetics, telecommunications and remote sensing from the University of Toulon-University of Nice Sophia Antipolis, Nice, France, followed by the Ph.D. degree from the University of Southampton, Southampton, U.K., on microwave radar remote sensing of the ocean at low grazing angles.

She has worked at the National Oceanography Centre for more than 20 years. Her interests include active and passive microwave remote sensing of the ocean, understanding interactions of microwave signals with the ocean surface, remote sensing of ocean wind and waves, and developing new earth observation technologies and applications. Her work includes research in altimetry for sea state, along-track interferometric SAR for currents, GNSS Reflectometry for surface winds and sea state, SAR altimetry, salinity from space with SMOS, and wide-swath ocean altimetry.

Giuseppe Foti received the M.Eng. degree in electronics engineering from the University of Catania, Catania, Italy, in 2000. He received the M.Sc. degree in oceanography from the University of Southampton, Southampton, U.K., in 2013.

In 2001, he joined the Communication Systems Section of the European Space Agency, Noordwijk, The Netherlands, where he conducted research in the field of spread-spectrum techniques for a packet access in broadband satellite systems. From 2003 to 2010, he served in the Principal Directorate of Telecommunications at the European Patent Office, Rijswijk, The Netherlands, as a Patent Examiner. In the same year, he joined the Satellite Oceanography section of the National Oceanography Centre, Southampton, U.K., where he currently works as a Research Scientist. His current research interest includes remote sensing of the oceans, with special emphasis on techniques using signals of opportunity (GNSS-R).

Mr. Josep Roselló received the Graduate degree in telecommunications engineering in 1991 from the Polytechnical University of Catalonia, Barcelona, Spain.

He started working in 1993 at ESTEC Technical Directorate in signal and data processing of earth observation and Galileo payloads. Since 2007, he has been with the Future Missions Division of the Earth Observation Directorate, and also at ESTEC. His current responsibilities include internal research and technical management of industrial and academic contracts, as well as interagency co-ordination. He is leading ESA in the deployment from LEO orbit of the data downlink in the 25.5 to 27 GHz k-band band and the development of new GNSS payloads for earth observation.